

DOI: 10.1002/cvde.200806747

Full Paper

Bridging Experiments and Simulations in Oblique Angle Polymerization

By Murat Cetinkaya and Melik C. Demirel*

In this paper, we report the growth of nanostructured poly(*p*-xylylene) (PPX) films by oblique angle polymerization at various deposition angles. Additionally, a two-dimensional computational (Monte Carlo) model is implemented to study the nanostructured growth process. The morphology of the nanostructured polymer films are characterized by atomic force microscopy and scanning electron microscopy. Based on the experimental results, a competitive growth model is proposed and quantified in terms of column geometry (i.e., diameter and height), column spacing (i.e., periodicity), and column packing (i.e., number of columns per unit area). We show that the nanostructured polymer growth obeys a universal power-law scaling mechanism at various deposition angles. The computational model predicts similar nanostructured morphologies to the oblique angle polymerization obtained experimentally. Nanostructured polymer films may provide great advances in sensing and biomedical applications.

Keywords: monte carlo simulation, oblique angle polymerisation, parylene, PPX, scaling

1. Introduction

Oblique angle deposition is widely studied because nanostructured morphologies are easily obtained with a single-step physical vapor deposition (PVD) method.^[1–4] A general observation from PVD studies is the power-law scaling of columnar morphology that formulates the growth of columns with allometric relationships.^[5–7] It has been noted that characteristic power-law values of columns (e.g., geometry, spacing, and packing) depend on the deposited material and the angle of the incoming flux.^[1]

Recently, we reported a novel process for depositing nanostructured polymers by oblique angle polymerization (OAP).^[8–10] OAP is a vapor deposition polymerization (VDP) method that creates a porous and low-density film of nanostructured columns. OAP starts with a monomer or a dimer, which is converted to a polymer during the growth process. OAP is different from conventional oblique angle deposition because the reactive monomer in OAP has to search for the end of the polymer chain after it has condensed on the surface. Therefore, particle diffusion rates in OAP are higher than in conventional PVD processes.

In this paper, we study the growth of nanostructured PPX films at three deposition angles by experimental and computational methods. The deposition angle (α) was crucial in column formation since a columnar morphology was observed only for $\alpha < 30^\circ$. The effects arising from OAP at three deposition angles were investigated experimentally

in terms of the lateral arrangement of columns on the substrate surface. Additionally, the OAP process was modeled by a two dimensional Monte Carlo (MC) model. The computational results from the chain algorithm agreed with the experimental results for nanostructured PPX films under certain simulation conditions. Power-law scaling of nanostructured PPX films was successfully modeled with the MC chain algorithm. The chain algorithm also indicated that PPX columns were composed of straight chains bundled along a column. Thus, the chain algorithm was found to be more suitable for the simulation of nanostructured PPX films. The experimental results for columnar PPX films are compared to the simulation results and the validity of our computational model is discussed.

2. Results and Discussion

We have studied the growth of nanostructured poly(dichloro-*p*-xylylene) (PPX-Cl) formed through vapor phase polymerization at three different deposition angles ($\alpha = 5, 10, \text{ and } 15^\circ$). Figure 1a shows a schematic of the nanostructured PPX-Cl film deposited by the OAP process. The substrate is tilted at an angle (α) with respect to the incident vapor flux (Fig. 1b), thereby exciting a self-shadowing^[10] and nucleation process.^[11] The columnar morphology of nanostructured PPX films constitutes a carpet of densely-packed fibers (i.e., 160 nm diameter; $\sim 10^7$ columns per mm^2). Figure 1c shows cross-sectional scanning electron microscope (SEM) images of a nanostructured PPX film and confirms the nanostructured morphology of the PPX film.

[*] Prof. M. C. Demirel, M. Cetinkaya
Department of Engineering Science and Materials Research Institute
The Pennsylvania State University, University Park, PA 16802 (USA)
E-mail: mdemirel@enr.psu.edu

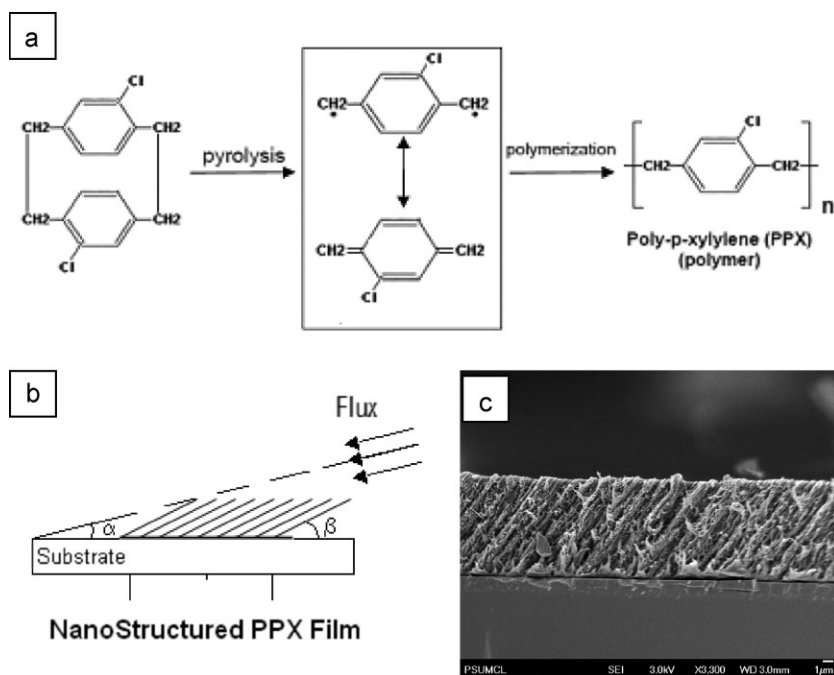


Fig. 1. a) Dichloro-[2.2]paracyclophane is converted to PPX-Cl polymer by radical polymerization. b) Schematic showing the preparation process for OAP-PPX films. c) A picture of the cross-sectional SEM image of a nanostructured polymer film ($\sim 10 \mu\text{m}$ thick) deposited at 15° via the OAP method.

The nanostructured PPX-Cl film was characterized using an atomic force microscope (AFM) to measure surface features (i.e., column diameter, spacing, and packing) at various film thicknesses. The measurement results showed that the average column diameter (d) scales as a function of column height (h) according to the power-law shown in Equation 1, where p is a characteristic value inherent to the

material and deposition conditions.

$$d \sim h^p \quad (1)$$

It has been reported that p values for non-polymeric materials can vary from 0.30 to 0.60.^[1] Another power-law relationship can be written between column height (h) and column number density (i.e. number of columns per unit area), as shown in Equation 2, where n is the column number density at height h , and p_n is the scaling exponent.

$$n \sim h^{p_n} \quad (2)$$

Tang et al.^[7] reported that p_n is approximately -1.0 for ruthenium columnar films. Similarly, spacing between columns can be expressed as a function of column height, as shown in Equation 3, where λ is the periodic spacing between columns at height h , and p_λ is the scaling exponent.

$$\lambda \sim h^{p_\lambda} \quad (3)$$

Tang et al.^[7] reported that p_λ is approximately 0.50 for ruthenium columnar films. Equations 2 and 3 indicate the existence of competitive growth among columns such that column number density (n) decreases and the periodic spacing between columns (λ) increases as column height (h) increases. Nanostructured PPX-Cl films obey power-law scaling with p values ranging from 0.11 to 0.27 (see Fig. 2) and p_n ranging from -0.18 to -0.53 . Table 2 shows the values for characteristic exponents for three different deposition angles. Theoretically, the substitution of Equation 2 into Equation 3 should give $p_\lambda = -\frac{1}{2}p_n$ (assuming $\lambda^2 \sim 1/n$). Therefore, the theoretical power ratio, p_λ/p_n is equal to -0.5 , which is in good agreement with the experimental data in Table 2.

We developed a two-dimensional Monte Carlo (MC) model to study OAP. The MC model is tested with two different deposition algorithms. A chain-based algorithm simulated depositing particles by incorporating them into growing chains. A non-chain algorithm simulated depositing particles by letting them cluster without any site restrictions as in the chain-based algorithm. The chain model emphasizes the significance of polymerization in oblique angle deposition. The deposition of particles with chain and non-chain algorithms is illustrated in Figure 3a. Briefly, all incoming particles have to diffuse “D” steps. In Figure 3a, the incoming directions for particles “1” and “2” are shown with solid arrows. A particle is allowed to diffuse along the substrate (e.g., particles “2” and “4”) or along the columns

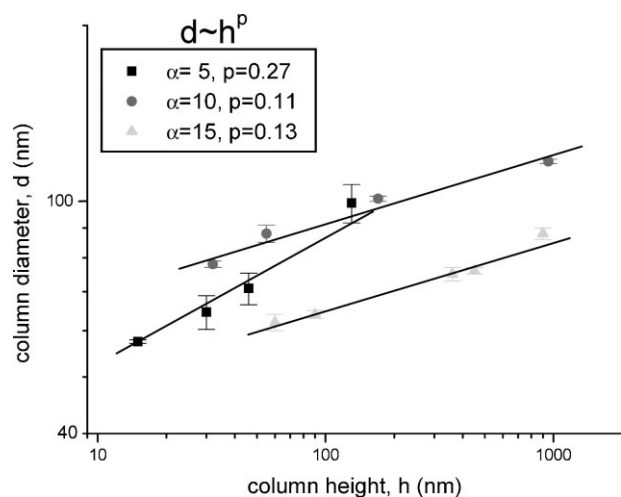


Fig. 2. Power-law scaling of columnar growth in nanostructured PPX-Cl films deposited at three different deposition angles, $\alpha = 5^\circ$, 10° , and 15° . Solid lines and error bars represent the best fits and standard deviations based on three sets of measurements, respectively. The thickness of the films deposited at $\alpha = 5^\circ$ spans a shorter range compared to other angles because we did not observe the nanostructured morphology for films which are thicker than ~ 200 nm.

Table 1. List of simulation parameters and calculated quantities. p , p_n , and p_λ are scaling exponents (see Eq. 1–3).

Simulation parameter	Symbol	Range of values	Calculated quantities
Model		Chain/non-chain	p, p_n, p_λ
Deposition rate (particles per step)	F	1–1000	p, p_n, p_λ, ν
Diffusion rate (steps per particle)	D	0–2000	p, p_n, p_λ, ν
Deposition angle (degrees from horizontal)	α	10–90	p, p_n, p_λ, ν
Diffusion acceptance parameter	T	0.1–100	p, p_n, p_λ

Table 2. Experimental values of p , p_n , and p_λ . (α is the deposition angle).

Film type	α	p	p_n	p_λ	$p_\lambda p_n$
PPX-Cl	5°	0.27 ± 0.01	−0.53 ± 0.01	0.27 ± 0.01	−0.51
	10°	0.11 ± 0.01	−0.18 ± 0.04	0.10 ± 0.01	−0.56
	15°	0.13 ± 0.01	−0.30 ± 0.01	0.17 ± 0.02	−0.57

(e.g., particle “3”) and can form overhangs, depending on the final particle position. Possible diffusion directions for particles “1–4” are indicated with dashed arrows. Particles follow diffusion directions for both chain and non-chain models. In addition, if the chain algorithm is selected, a particle will join an existing chain by incorporation through the chain ends (indicated with grey beads). For instance, particles “1–4” have a chance of joining one of the existing chains depending on their diffusion direction. Two coincid-

ing monomers can also form a new chain as shown by particles “5” and “6” for the chain model.

The MC simulation generated morphologies are similar to the nanostructured PPX films observed experimentally. Particles are deposited at a tilting substrate (see Fig. 3b). The tilt angle is equal to $90-\alpha$. At the end of the simulation, the substrate was tilted back to the horizontal position for visualization purposes. Simulations with chain and non-chain algorithms produced certain differences (see Fig. 3c). The chain algorithm produced porous and fibrous columns. On the other hand, films simulated with the non-chain algorithm are composed of densely packed and aligned columns. Figure 3c shows a snapshot from a simulation in which the chain algorithm is switched on at an intermediate height. During non-chain simulation, the columns are compact due to close packing of incoming particles. After the activation of the chain-based algorithm, the morphology is shifted to entangling branches due to the formation and growth of polymer chains.

When considering polymeric films, the conformation of polymer chains is another important quantity that may provide insight to the film morphology. Polymer chain conformation is calculated by using Equation 4,^[12,13] where L_c is the polymer chain length, $\langle R^2 \rangle^{1/2}$ is the root-mean-square end-to-end distance of a chain, and ν is the scaling exponent for chain conformation (see Fig. 4a).

$$\langle R^2 \rangle^{1/2} \sim L_c^\nu \quad (4)$$

Considering an ideal polymer chain formed via a self-avoiding walk (see the literature^[12,14]), the scaling exponent for chain conformation, ν , is equal to $3/(2+d_s)$, where d_s is the dimensionality of the system.^[14] The scaling exponent for an ideal polymer chain, ν , is equal to 0.75 for a two-dimensional system. On the other hand, $\nu=1$ indicates a fully extended polymer chain. MC simulations performed with the chain-based algorithm showed that the average value of the scaling exponent ν

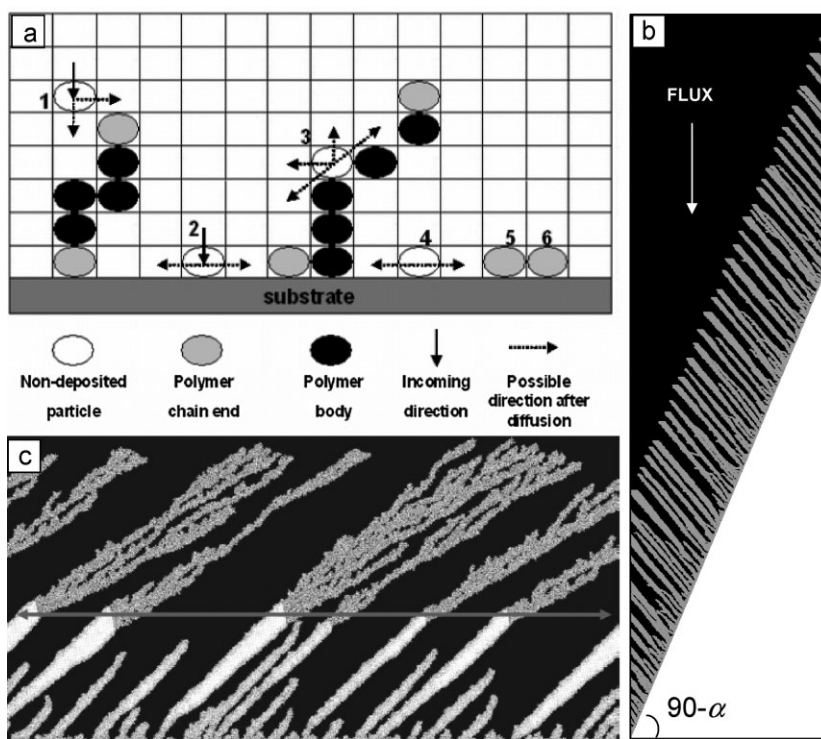


Fig. 3. a) Illustration of the deposition algorithms for polymeric and non-polymeric particles. b) Orientation of the substrate during deposition. In this example, the substrate is tilted at $\delta = 90 - \alpha = 70^\circ$ from the horizontal at a deposition angle $\alpha = 20^\circ$. c) Snapshot from a simulation where the polymer algorithm is switched on at an intermediate height (indicated by the arrow).

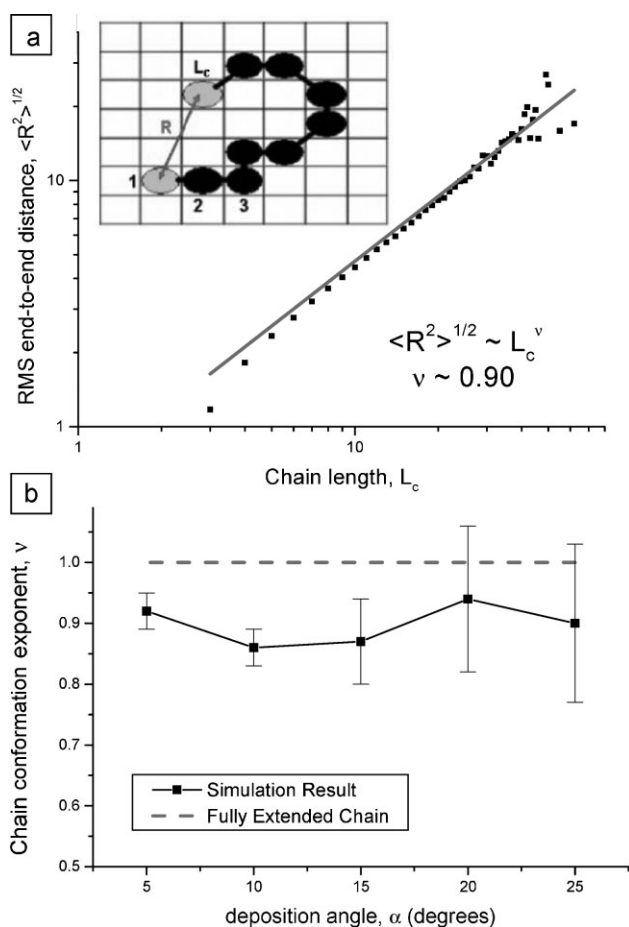


Fig. 4. a) Log-log plot of rms end-to-end distance $\langle R^2 \rangle^{1/2}$ is plotted as a function of chain length L_c for deposition angle $\alpha = 10^\circ$. The inset shows the illustration for a simulated polymer chain. The solid line shows the best fit for a power-law relationship. b) Chain conformation exponent v at various deposition angles, α . The dashed line indicates v for a fully extended chain. Simulation parameters for both figures are diffusion $D = 500$, deposition rate $F = 500$, and acceptance rate $T = 1$.

is equal to 0.90. As shown in Figure 4b, v varies between 0.86 and 0.94 at various deposition angles, α .

We compared the experimentally measured column spacing p_λ to MC simulation results (Fig. 5). The films were deposited at three different depositing angles ($\alpha = 5, 10, \text{ and } 15^\circ$). The scaling exponent p_λ is a direct measure of the competitive growth process. It is possible to calculate the maximum shadowing length L_s for the OAP based on the deposition angle geometry, using Equation 5, where h is the height of a column.

$$h / \tan(\alpha) = L_s \quad (5)$$

The shadowing length (L_s) determines the column separation assuming a uniform vapor flux. Larger shadowing lengths (i.e., lower deposition angle) should lead to lower p_λ values, indicating that competitive growth is less effective

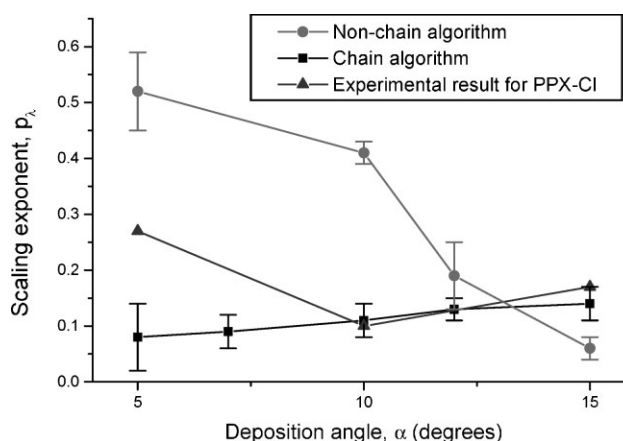


Fig. 5. The scaling exponent, p_λ , is shown as a function of deposition angle, α , for simulation results (chain and non-chain algorithms) and experimental results (PPX-CI). Error bars represent standard deviations based on multiple simulation results (i.e., random seed for M.C. simulation).

with increasing distance between nucleating columns on a substrate. However, we should also note that diffusion becomes important as the column packing is increased. Consequently, the discrepancy between computational and experimental results for nanostructured PPX films is larger at small deposition angles.

3. Conclusions

Both experimental and simulation results showed that columnar films deposited by OAP obey power-law scaling. The magnitudes of the scaling exponents depend strongly on the deposition angle and simulation algorithm. We presented two simulation models for OAP (chain and non-chain). An important factor in columnar growth is the deposition angle. The chain-based deposition algorithm predicted the experimentally observed nanostructured PPX growth at 10° and 15° , whereas there is discrepancy in both non-chain and chain models at 5° . Although the simulation results are in good agreement with the experimental observations at 10° and 15° , there is a discrepancy between experimental and computational results at 5° . This may be attributed to a simplistic two-dimensional model which may not be realistic. Other parameters, such as chain conformation on column geometry (i.e., entropic effects) and chain-chain interaction require further elucidation in the simulation for an accurate prediction.

OAP provides a novel process for creating nanostructured polymers. Understanding the growth and formation of nanostructured polymers will provide significant progress toward the development of new three-dimensional functionalized surfaces for medical and engineering applications.

4. Experimental

The deposition of columnar poly(chloro-*p*-xylylene) (PPX-Cl) films by oblique angle polymerization was described in our previous work [15]. Briefly, the dimer precursor dichloro-[2.2]paracyclophane was placed in a vacuum chamber and converted to a reactive gas of monomers by pyrolysis (690 °C). Glass and silicon substrates were used, and cleaned with acetone and isopropanol prior to deposition. The substrate was held fixed in a tilted orientation relative to the incoming vapor. The vapor pressure in the deposition chamber was maintained at approximately 10–20 mTorr. The deposition process was completed 10 min after the required vacuum level had been achieved. Film thickness (i.e., column height) was measured with a Tencor P10 profilometer. The scanning parameters for the profilometer were as follows: the scan speed was 20 μm s⁻¹, the stylus force was 9.8 μN, and the sampling rate was 200 Hz.

Surface characterization of columnar PPX-Cl films was performed with a Nanoscope-E AFM (Veeco Metrology, CA). Topography images are collected in ambient air at room temperature using silicon nitride (SiN) triangular cantilevers in the contact mode (DNP Series, $k=0.58$ N m⁻¹, Veeco Metrology, CA). AFM topography images were acquired with Nanoscope Software (Veeco Metrology, CA). Each measurement was replicated three times and the average results presented. AFM topography images are modified with the “highpass” filter tool of Nanoscope Software prior to further analysis. The highpass filter calculates the weighted difference between a pixel in the image and its eight neighbors. This data point was then replaced by the calculated difference. This operation is useful for highlighting the edges of the columns. Image quality was kept at 256 pixels × 256 pixels.

Column periodicity was calculated using the two dimensional power spectral density (PSD) function, shown in Equation 6.

$$PSD = \frac{1}{A} \left| \frac{1}{2\pi} \int dx \int e^{i(ux+vy)} h(x,y) dy \right|^2 \quad (6)$$

$h(x,y)$ is the height at a location (x,y) , u and v are frequencies in the x and y directions, and A is the scanned area. Here, PSD is a function of the lateral frequencies u and v , and the integrations are performed over all data points (x,y) on the surface. If the surface is isotropic, a single frequency $f = [u^2 + v^2]^{1/2}$ can be evaluated in the PSD function. The peak PSD frequency (f_{max}) and the corresponding peak wavelength ($\lambda = 2\pi/f_{max}$) were estimated by fitting a Gaussian curve to the experimental PSD data points. By definition, the peak PSD wavelength shows the periodic spacing between dominant surface features. Therefore, the peak PSD wavelength refers to the periodic column spacing in nanostructured PPX films. PSD calculations were completed with Nanoscope Software using 5 μm surface scans of columnar PPX-Cl films.

Computational: The OAP process was modeled using a two dimensional Monte Carlo (MC) method. The simulation parameters of the MC method are listed in Table 1. All simulations were completed using 1.5×10^6 particles on 2000×1000 grids. The output files of MC simulation were visualized using ImageJ software [16].

In the MC model, incoming particles are simultaneously sent in a vapor flux and they diffuse a certain number of steps prior to deposition. Particles are incorporated into the growing film according to two different deposition algorithms. A chain-based algorithm incorporates diffusing particles into growing linear chains. A non-chain algorithm on the other hand, does not restrict particle deposition and therefore allows the clustering of particles in a closed packed fashion. A periodic boundary condition was used for particles moving along the substrate surface. The results pertaining to film morphology were recorded at periodic intervals of film height and moving average values were used in calculations, as shown in Equation 7, where j is the current number of data points and x_i is the raw i^{th} data value with $1 \leq i \leq j$.

$$\langle x_j \rangle = \frac{1}{j} \sum_{i=1}^j x_i \quad (7)$$

Received: September 29, 2008

Revised: January 5, 2009

- [1] C. Buzea, G. Beydaghyan, C. Elliott, K. Robbie, *Nanotechnology* **2005**, *16*, 1986.
- [2] T. Karabacak, J. P. Singh, Y. P. Zhao, G. C. Wang, T. M. Lu, *Phys. Rev. B* **2003**, *68*, 5.
- [3] R. J. Martin-Palma, J. V. Ryan, C. G. Pantano, *J. Appl. Phys.* **2007**, *101*, 5.
- [4] G. Xia, S. Wang, H. B. He, K. Yi, J. D. Shao, Z. X. Fan, *J. Alloys Compd.* **2007**, *431*, 287.
- [5] K. Kaminska, A. Amassian, L. Martinu, K. Robbie, *J. Appl. Phys.* **2005**, *97*, 013511.
- [6] T. Karabacak, G. C. Wang, T. M. Lu, *J. Appl. Phys.* **2003**, *94*, 7723.
- [7] F. Tang, T. Karabacak, L. Li, M. Pelliccione, G. Wang, T. Lu, *J. Vac. Sci. Technol. A* **2007**, *25*, 160.
- [8] M. Cetinkaya, S. Boduroglu, M. C. Demirel, *Polymer* **2007**, *48*, 4130.
- [9] M. C. Demirel, M. Cetinkaya, A. Singh, W. J. Dressick, *Adv. Mater.* **2007**, *19*, 4495.
- [10] M. Cetinkaya, N. Malvadkar, M. C. Demirel, *J. Polym. Sci. Part B* **2008**, *46*, 640.
- [11] M. C. Demirel, A. P. Kuprat, D. C. George, G. K. Straub, A. D. Rollett, *Interf. Sci.* **2002**, *10*, 137.
- [12] W. Bowie, Y. Zhao, *Surf. Sci.* **2004**, *563*, L245.
- [13] T. Nishida, K. Yasumoto, T. Otori, J. Desaki, *Invest. Ophthalm. Vis. Sci.* **1988**, *29*, 1887.
- [14] P. Meakin, *Phys. Rev. A* **1988**, *37*, 2644.
- [15] S. Boduroglu, M. Cetinkaya, W. J. Dressick, A. Singh, M. C. Demirel, *Langmuir* **2007**, *23*, 11391.
- [16] M. Abramoff, P. Magelhaes, S. Ram, *Biophoton. Intern.* **2004**, *11*, 36.